Scattering of Electromagnetic Waves in Hypersonic Plasma: Numerical Simulations and Analysis

Scattering of Electromagnetic Waves in Hypersonic Plasma: Numerical Simulations and Analysis

Salvatore Esposito* and Domenic D'Ambrosio†
Politecnico di Torino, Dipartimento di Elettronica e Telecomunicazioni (DET), Torino, 10129, Italy
Politecnico di Torino, Dipartimento di Ingegneria Meccanica e Aerospaziale (DIMEAS), Torino, 10129, Italy

Andrea Scarabosio‡
LINKS Foundation, Torino, 10138, Italy

Giuseppe Vecchi§
Politecnico di Torino, Dipartimento di Elettronica e Telecomunicazioni (DET), Torino, 10129, Italy

This paper presents a study on the scattering of electromagnetic waves in the plasma field surrounding hypersonic vehicles. The research focuses on analyzing the radar cross-section (RCS) of a cone-shaped blunt body under various suborbital altitudes (20 to 70 km) and Mach numbers (8 to 16) conditions. Computational Fluid Dynamics (CFD) analysis is employed to evaluate characteristic quantities of the plasma field, such as the electron plasma frequency, collision frequency, and permittivity. This work considers a collisional, inhomogeneous, and cold plasma electromagnetic wave propagation model. It uses two different approaches, namely an asymptotic ray-tracing model and a full-wave finite-difference time-domain (FDTD) method, to compute the radar cross-section (RCS). Noticeable variations in the RCS induced by the plasma are observed, particularly in scenarios with elevated Mach numbers. This research provides insights into the complex interactions between electromagnetic waves and plasma in hypersonic flight conditions, contributing to the understanding of plasma-induced disturbances on radar systems.

I. Introduction

Hypersonic flight is a challenging condition that presents significant difficulties in the design of flight vehicles and operations. This flight regime is typical for aircraft reentering Earth's atmosphere from various orbits or entering extraterrestrial atmospheres (for example, on Mars). It is also typical for meteors and space debris that deorbit and need to be monitored for safety reasons[1, 2]. Objects moving at speeds much greater than the speed of sound (typically a Mach number M>5) transfer a significant amount of kinetic energy to the surrounding gas through a shock wave detached from the body. This leads to an increase in the internal energy of the gas and the formation of a high-temperature region around the body [3]. Due to the high-temperature effects, the gas properties undergo significant changes compared to supersonic and subsonic flight regimes.

The high temperatures trigger chemical reactions within the flow field, resulting in the generation of new species. Thus, the air becomes a chemically reactive gas mixture, subject to dissociation phenomena and ionization if the temperature permits. When ionization occurs, the body becomes enveloped in plasma with a significant trailing wake. The presence of free electric charges (electrons and ions) in the plasma strongly influences the behavior of electromagnetic (EM) waves, with the electron plasma frequency reaching beyond several GHz, and can even lead to complete wave propagation blockage and reflection (cut-off condition)[4].

This research aims to study the scattering of EM waves in the plasma field by calculating the radar cross-section (RCS) for suborbital hypersonic flight vehicles. A cone-shaped blunt body [5] will be used for the study, and its behavior in hypersonic flight will be simulated under a variety of suborbital altitude and Mach number settings with an axial

*Ph.D. Student, Politecnico di Torino, Dipartimento di Elettronica e Telecomunicazioni (DET), Corso Duca degli Abruzzi, 24, Torino, 10129, Italy.

†Adjunct Professor, Politecnico di Torino, Dipartimento di Ingegneria Meccanica e Aerospaziale (DIMEAS), Corso Duca degli Abruzzi, 24, 10129 Torino, Italy.

‡Scientific Researcher, LINKS Foundation, Via P.C. Boggio, 61, 10138 Torino, Italy.

§Full Professor, Politecnico di Torino, Dipartimento di Elettronica e Telecomunicazioni (DET), Corso Duca degli Abruzzi, 24, 10129 Torino, Italy.

symmetry condition. To achieve this, a test matrix will be created, encompassing Mach number values ranging from 8 to 16 and altitudes ranging from 20 to 70 km. Despite its straightforward nature, this geometric arrangement offers a solid framework for studying the formation of plasma surrounding a slender object during atmospheric hypersonic flight.

The evaluation of characteristic quantities of the plasma field will be conducted using Computational Fluid Dynamics (CFD) analysis. Parameters including plasma electron frequency, plasma collision frequency, and permittivity will be employed in studying the RCS. Both an approximate asymptotic approach (ray-based) and a full-wave (exact Maxwell's equations) Finite-Difference Time-Domain method will be employed to examine the radar response.

II. Plasma model

A. Computational geometry and CFD model

Hypersonic Radio Frequency (RF) testing relies on Computational Fluid Dynamics (CFD) analysis to account for the distribution of physical quantities, such as permittivity and electron plasma frequency, in the flow field formed by the hypersonic vehicle. Since the flight regime is suborbital, the fluid is approximated as continuous and described by the Navier-Stokes equations for multi-component gas mixtures. In this study, the air is modeled as a compressible and chemically reactive mixture consisting of seven chemical species: oxygen (O_2), nitrogen (N_2), nitrogen oxide (NO), atomic nitrogen (N), atomic oxygen (O), nitrogen oxide ions ($NO+$), and electrons (e^-). The chosen physical model considers chemical reactions, ionization, and non-equilibrium phenomena, including vibrational and electronic energy relaxation. Specifically, a two-temperature model is used to describe non-equilibrium energetic effects. The thermodynamic properties of each chemical species are obtained from [6], while the chemical reaction rates are taken from [7, 8].

Overall, the body is 1.125 meters long. A 5.5 cm major radius and a 2.5 cm minor radius characterize the ellipsoid cone's nose. This is followed by a 2.5 cm long cylindrical segment, and at the end is a cone as described in [9], with a semi-opening angle of 8.2047°. Though basic, this geometric arrangement provides a good basis for modeling plasma generation around a thin body during hypersonic atmospheric flight. Beyond the nose, the computational domain extends up to 2.875 m in order to capture the plasma in the wake. The geometry of the cone is displayed in Fig 1.

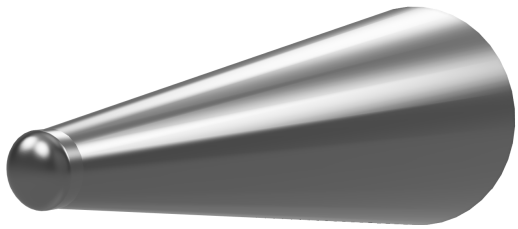

Fig. 1 Body Geometry

The main thermochemical activity occurs near the nose of the vehicle, where the shock wave is perpendicular to the direction of flow, resulting in higher temperatures and flow compressions. To capture the detailed effects of the bow shock, an adaptive mesh is employed, implementing grid refinements based on the magnitude of the Mach number gradient. An example is provided in Fig. 2.

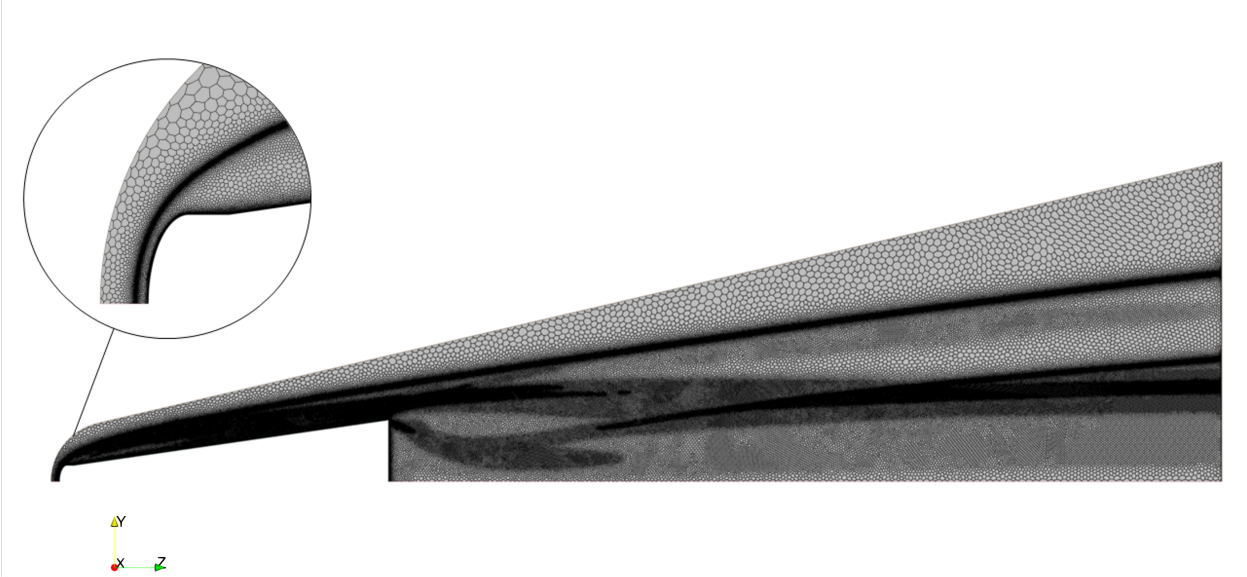

Fig. 2 Refined Grid at an altitude of 50 km and at a Mach number of 16.

All computations were performed using the commercial software CFD++.19.1, which is a solver based on the Navier-Stokes equations capable of simulating both compressible and incompressible fluid flow[10]. It employs a second-order Total Variation Diminishing (TVD) limited discretization scheme built upon a multi-dimensional interpolation framework. For this study, a Riemann solver [11] was employed to compute the upwind fluxes. The simulations conducted were steady Reynolds-averaged Navier-Stokes (RANS) simulations utilizing an SST $k-\omega$ turbulence model [12]. The characteristic convective time t_c for each simulation, defined as the length of the cone on the free stream velocity, ranges approximately from 3×10^{-4} to 5×10^{-4}. The equations are solved using an implicit temporal scheme with a time step $\Delta t = \frac{t_c}{50}$ to reach convergence. Each simulation has a duration of 600 t_c, which is sufficient to obtain converged simulations, also in terms of the chemical composition in the wake.

B. EM model

This study assumes that the medium remains stationary, while the electromagnetic fields exhibit a time variation expressed as $e^{i\omega t}$, where $\omega = 2\pi f$ represents the angular frequency corresponding to the frequency f. We are interested in frequency ranges where the plasma response is dominated by electron motion. The effects of collisions and neutral species in the plasma will be considered. However, as long as the phase velocity of the wave is much greater than the thermal velocity of the plasma, temperature effects and higher-order collective kinetic effects can be neglected. Therefore, a condition of collisional, unmagnetized, inhomogeneous, and cold plasma is considered, and its constitutive relation can be characterized using the Drude model[4]:

$$\epsilon_r(\mathbf{r}) = 1 - \frac{\omega_p^2(\mathbf{r})}{(\omega(\omega - i\nu_c(\mathbf{r}))} = 1 - \frac{\omega_p^2(\mathbf{r})}{(\omega^2 + \nu_c^2(\mathbf{r}))} + i\frac{\omega_p^2(\mathbf{r})\nu_c}{\omega(\omega^2 + \nu_c^2(\mathbf{r}))} \tag{1}$$

In this relation, ω is the link angular frequency, and ω_p is the electron plasma frequency defined by the following equation:

$$\omega_p(\mathbf{r}) = \sqrt{\frac{n_e(\mathbf{r})e^2}{m_e\epsilon_0}} \tag{2}$$

Here, n_e is the electron number density, e is the electron charge, m_e is the electron mass, and ϵ_0 is the vacuum permittivity. The neutral-plasma collision frequency ν_c is determined by the following formula[13]:

$$\nu_c(\mathbf{r}) = \sum_{i=1}^{N} n_i(\mathbf{r})\sigma_{i,e}\sqrt{\frac{8k_bT_e(\mathbf{r})}{\pi m_e}} \tag{3}$$

In Eq.(3), T_e represents the electron temperature, n_i is the number density of the i-th neutral species, $\sigma_{i,e}$ is the neutral-electron scattering cross-section for the neutral species i, and k_b is the Boltzmann constant. The cross-sections are taken from [6], while the number density values of the species and the electron temperature are outputs of CFD simulations.

When the electron density is high enough and the plasma frequency is equal to or greater than the link frequency, the real part of the permittivity might be null or even negative. The traveling EM wave becomes evanescent and rapidly (exponentially) loses intensity as it propagates through the affected regions of space. As a result of this phenomenon, the plasma surface effectively replaces the body's surface and reflects radiation, distorting the radar trace. Refraction and absorption can also take place even when the plasma frequency is below the cut-off values ($\nu_c \rightarrow 0$ and $\frac{\omega_p}{\omega} \geq 1$), causing a redistribution of electromagnetic waves and a reduction in re-radiation.

The propagation of the wave is governed by the real part of the permittivity, while the imaginary part determines the collisional absorption, which involves the transfer of energy from EM-wave energized electrons to neutrals.

To evaluate RF scattering (RCS), two methods will be adopted:

- Ray-tracing method[14]: These techniques are typically used to approximate plasma propagation using the Eikonal Ansatz, focusing specifically on the plasma region. The fields just outside the plasma region are accurately computed using the Radiation Integral[15–17]. The initial source or patterns are decomposed into plane waves carried by each ray, enabling effective management of propagation along the plasma cloud and reflection on vehicle surfaces. A custom code has been developed for this approach. In this work we will adopt the method only to compare the results in the case of a vacuum space scenario.
- Full-wave techniques: These methods involve numerically solving Maxwell's equations without any approximations. Among full-wave techniques, the Finite-Difference Time-Domain (FDTD) method is utilized due to its flexibility in the propagation medium model and relatively low computational cost, particularly in terms of memory requirements compared to other methods[18]. For this method, the commercial software CST Studio Suite has been employed[19].

III. Results

A. CFD Results

The results obtained from the CFD analysis were derived under conditions of non-catalytic and radiation-adiabatic walls, maintaining a zero angle of attack to ensure an axisymmetric flow. Employing a radiation-adiabatic wall boundary condition implies that the wall is considered adiabatic, yet it can radiate the heat received from the flow, a state known as 'radiative equilibrium'. This assumes that the gas is fully transparent to the radiation flowing away from the wall, while the wall benefits from radiative cooling. Previous research has established that, in numerous scenarios, this condition provides a reasonably accurate estimate of surface temperature compared to flight data [20]. The surface emissivity is assumed to be equal to 0.8 in this work.

For purely illustrative purposes and to maintain a certain level of simplicity, only the CFD results from a singular flight condition will be presented. Specifically, these results pertain to a condition significant for plasma formation, corresponding to a Mach number of M = 16 and an altitude of z = 50 km.

The images in Fig. 3 and Fig. 4 depict the values of plasma and collision frequencies in the flowfield. It is observed how a layer of plasma envelops the body, extending into the wake and affecting a region larger than the body itself. The plasma frequency values are on the order of GHz not only in the nose region, where the shockwave is more intense, but also across the rest of the body and part of the wake. In contrast, the collision frequency reaches GHz values only at the nose and exhibits values on the order of MHz in the remaining part of the plasma envelope. Figure 5 shows the real part of the relative permittivity field, which is revealed to be strongly inhomogeneous as expected. To enhance understanding, the illustration depicts two ranges of permittivity values, which have been computed considering a link frequency of $f = 1GHz$. The outcomes indicate that the real part of the permittivity reaches negative values near the body, whereas the wake exhibits permittivity values less than 1. Observing Fig.6, the highest values of the imaginary part of the permittivity are limited to the nose region, where the most intense thermochemical activity occurs, anticipating a negligible effect of collisional absorption.

For this flight condition, the findings forecast a redistribution of the RCS due to the presence of plasma compared to the vacuum case.

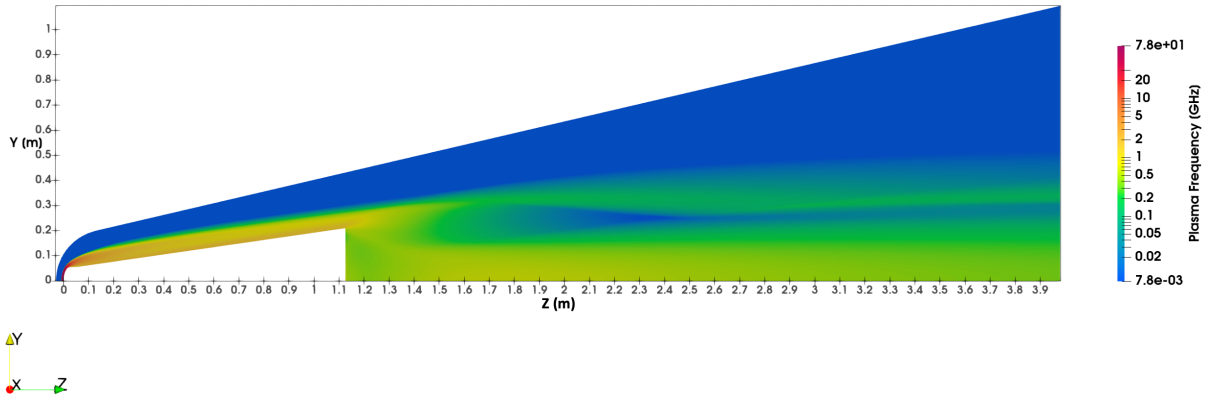

Fig. 3 Plasma Frequency at an altitude of 50 km and a Mach number of 16.

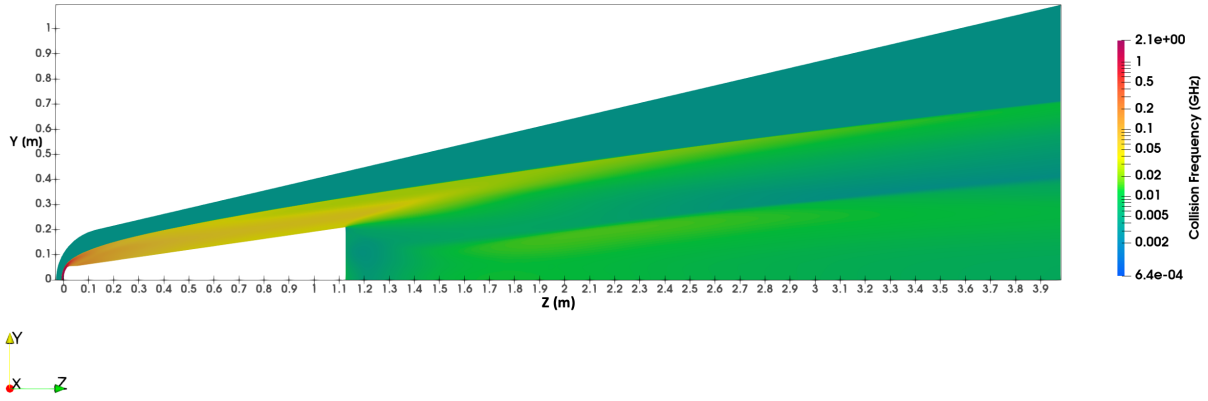

Fig. 4 Collision Frequency at an altitude of 50 km and a Mach number of 16.

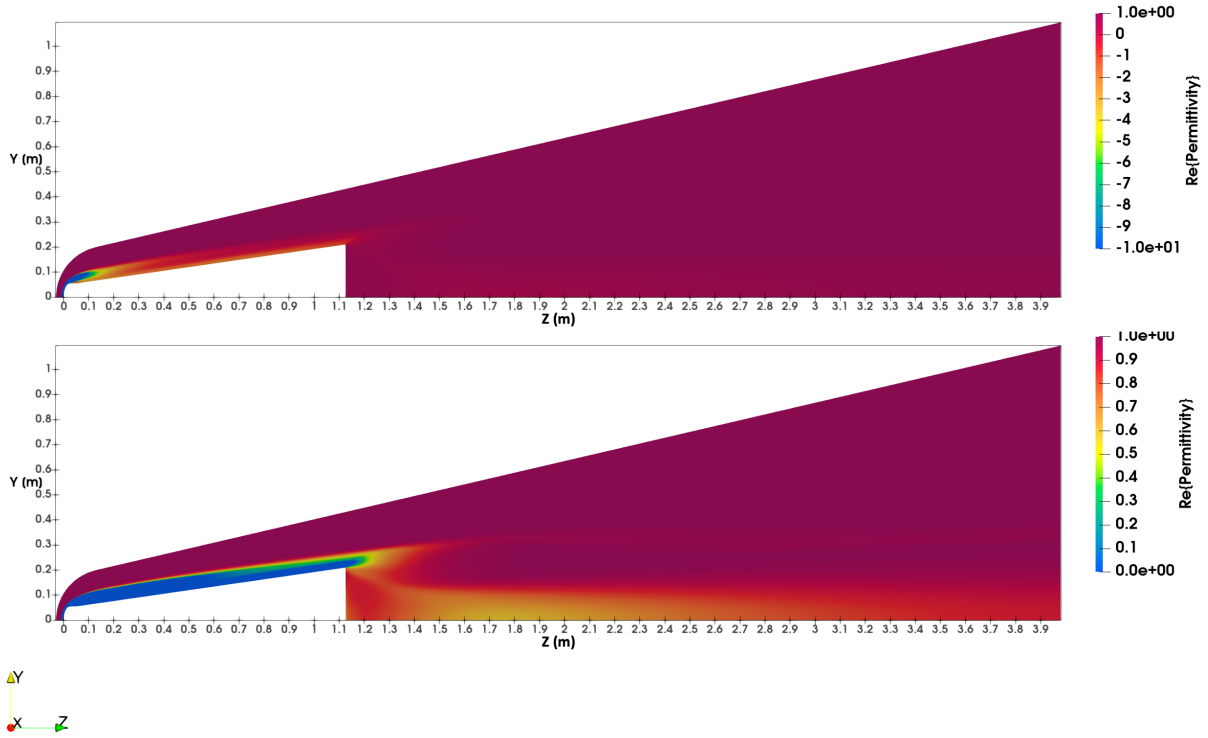

Fig. 5 Real part of permittivity at an altitude of 50 km and a Mach number of 16.

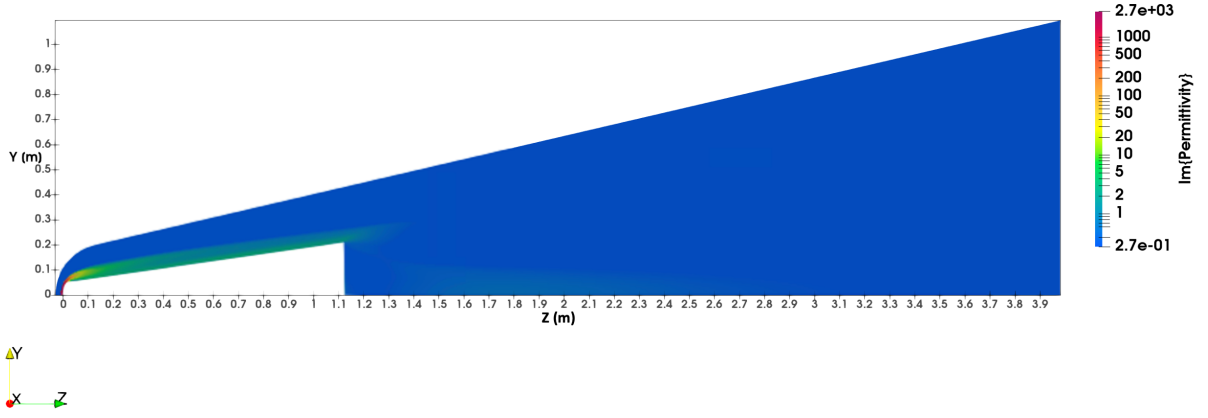

Fig. 6 Imaginary part of permittivity at an altitude of 50 km and a Mach number of 16.

Finally, Tab. 1 reports the maximum wall temperatures for various Mach and altitude conditions obtained through these CFD analyses. Flight conditions identified as unviable due to thermal protection concerns have been excluded. Setting the maximum temperature for the vehicle surface at 3500 K, Tab.1 highlights the infeasibility of Mach 14 and 16 conditions at 20 km altitude, along with the Mach 16 condition at 30 km altitude. The results also reveal that no high-temperature effects are observed at an altitude of 70 km for Mach numbers between 8 and 10. The poor thermochemical activity is attributed to the low density and pressure characterizing this altitude, and therefore, these observations will not be reported.

z[Km]\M	8	9	10	12	14	16
70	/	/	/	1.47E+03	1.68E+03	1841
50	1.56E+03	1.74E+03	1.91E+03	2.05E+03	2.27E+03	2.51E+03
30	2041	2.30E+03	2.43E+03	2.82E+03	3.29E+03	3.76E+03
20	2.25E+03	2.43E+03	2.83E+03	3.34E+03	3.84+E03	4.44E+03

Table 1 Maximum wall temperature in Kelvin degrees.

B. CEM Results

All electromagnetic analyses were conducted at a frequency of 1 GHz, considering the cone as a perfect electric conductor (PEC). This is a good approximation in the absence of knowledge about materials composing the body and significantly simplifies the analysis of scattering phenomena, making Maxwell's equations easier to solve [21]. The selection of this particular electromagnetic wave frequency is motivated by its practical significance in radar surveillance applications. It also serves the purpose of facilitating a meaningful comparison between asymptotic methods, applicable at high frequencies, and full-wave methods, all without necessitating an excessive computational effort for the latter.
Before looking at the plasma case, we establish a baseline comparison between full-wave and asymptotic methods in vacuum. The results of bistatic RCS are reported in this section and in the reminder of the manuscript as cut at $\phi = 90$ since the wave-vector of the incident lies always in the $y - z$ plane. In Fig. 7 we show the RCS for both horizontal (left) and vertical (right) linear polarization obtained considering an electromagnetic plane-wave incident at an angle relative to the cone axis of θ = -135°. For this comparison, shallow angles of incidence are intentionally avoided because of the well-known difficulties of the asymptotic methods to accurately reproduce the diffractive effect when dealing with conical shapes, but they become more reliable at larger angles. Therefore, the case of θ = -135° was specifically chosen to evaluate the consistency and conformity of the results. Figure 7 presents the RCS as a function of the observation angle, and the inset offers a clear visualization of the observation setup, emphasizing the angle at which the electromagnetic wave strikes the cone. These results pertain to the vacuum space condition, where, alongside our custom ray-tracing (RT) method and the previously mentioned FDTD approach, additional techniques are accessible within the CST software. Specifically, the supplementary methods employed include an integral equations (IE) solver, a full-wave solver utilizing the method of moments (MOM) technique with the multilevel fast multipole method (MLFMM) [22], and the asymptotic Shooting and Bouncing Rays (SBR) technique [16].
First of all, we notice the excellent agreement between both full-wave methods (FDTD and the integral solver). Similarly, the two asymptotic methods (custom ray-tracing and SBR) agree very well, as expected. Comparing full-wave and asymptotic results, the resemblance between findings is significant, showcasing a similar trend. Upon examination of the figure, it becomes apparent that the values of the two main peaks, namely the reflected peak (θ about -60°) and the forward scattering peak (θ = 45°), consistently align across all the methods employed. It is important to underline that the reflected peak is not at θ = -45°, as one would expect, but is shifted towards -60° due to the cone's semi-aperture angle of approximately 8.2°. Larger discrepancies arise in the angular region around the nose of the cone body, where lower RCS values are observed. Of particular interest, is the back-scattering or return radar at θ = -135°, which is weak here, showing a larger variation across the various methods in the range of $-14/-19$ dBsm. The large diffractive

contribution in this angular region makes an accurate evaluation difficult for the full-wave methods as well. Another noticeable difference is apparent when comparing the effect of wave polarization. The asymptotic approaches show a weak polarization dependence basically across the entire angular range except near the polar axis (here z-axis in Cartesian coordinate), whereas in the full-wave results both main peaks are larger for vertical polarization. Again these differences are attributed to diffraction.

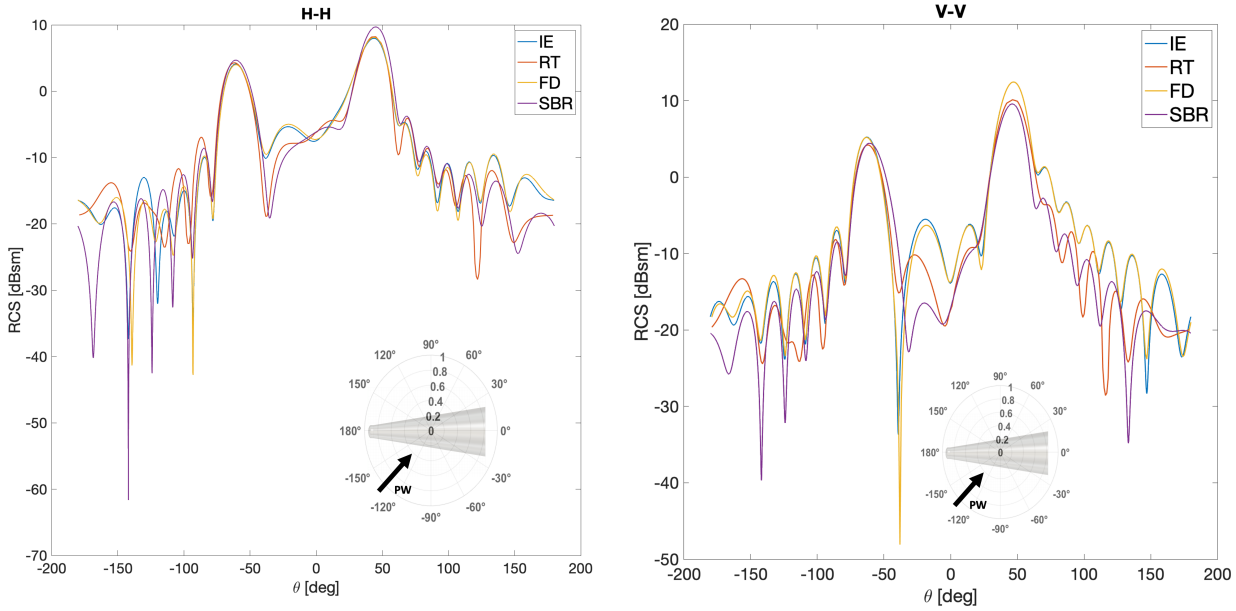

(a) Horizontal polarization **(b) Vertical polarization**

Fig. 7 Bistatic RCS comparison for a vacuum scenario

For the anaylsis conducted in presence of plasma, we present FDTD results calculated with horizontal polarization only. In Fig. 8, the results derived from FDTD simulations during the test campaign are presented, encompassing Mach numbers ranging from 8 to 16, altitudes from 20 to 70 kilometers, and an incidence of EM wave of -135°. The figure depicts two scenarios: the vacuum space condition is represented by the black line, the red line signifies a plasma modeled using the Drude model. At Mach numbers below 10, plasma has a minor impact on RCS distribution, except for a slight increase in forward scattering due to the presence of the wake. However, as Mach numbers exceed 10, the increased degree of ionization from the more intense shock wave makes plasma effects on electromagnetic scattering and RCS distribution non-negligible.

Observing the altitude effect, a change in RCS is appreciable at 20 kilometers from Mach number 10 onward. Yet, practical limitations hinder flight beyond Mach 12 due to excessively high wall temperatures. At 70 km of altitude, where free-stream air pressure and density are extremely low, a Mach number of 16 is necessary to ionize the fluid and significantly affect the RCS. Between 30 and 50 kilometers altitude, Mach numbers exceeding 10 induce plasma density and distributions impactful enough to considerably alter RCS. Moreover, as the Mach number increases, there is a more pronounced effect on the redistribution of RCS due to plasma compared to the vacuum case, which is coherent with expectations. This observed phenomenon is associated with an augmented ionization rate resulting from the more intense shock wave as the Mach number increases. The formed plasma is subsequently convectively transported into the wake, resulting in a higher plasma density everywhere. These findings highlight that the impact of plasma on electromagnetic scattering extends over a much larger region than the body itself, and the long plasma wake must be taken into account for RCS considerations.

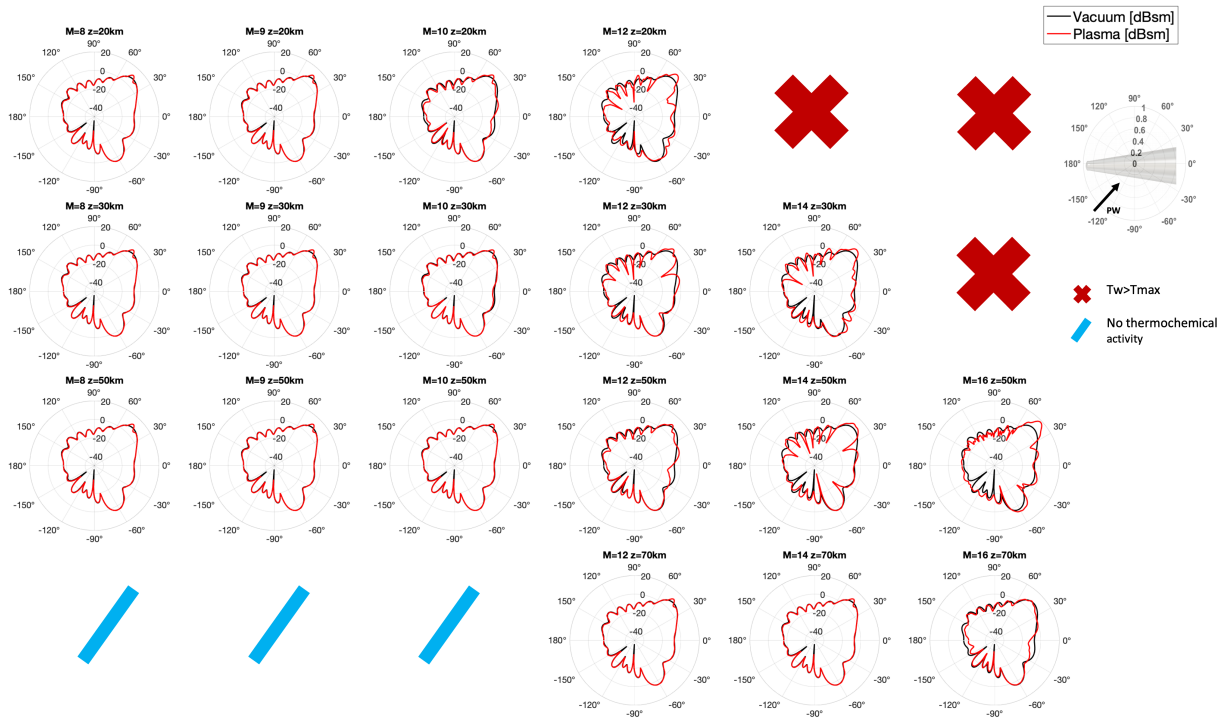

Fig. 8 Plasma Effects on RCS for different altitude and Mach number conditions

IV. Conclusions

This research focused on analyzing the impact of plasma on electromagnetic scattering, with particular attention to the complexities introduced by high temperatures and plasma formation in hypersonic flight conditions. The main objective was to investigate the RCS of suborbital hypersonic vehicles, using a cone-shaped blunt body as a representative model. The plasma field around the body and its properties were thoroughly examined through computational fluid dynamics (CFD) analysis, considering a viscous, compressible, and chemically reactive mixture comprising seven species. To evaluate the interaction of electromagnetic waves with the plasma sheath, a collisional, unmagnetized, inhomogeneous, and cold plasma model was adopted. Two different methods, ray-tracing and finite-difference time-domain (FDTD), were employed to compute the RCS. The electromagnetic analysis exhibited consistent trends in RCS between different methods in a vacuum environment. A comprehensive survey of RCS under various hypersonic flight conditions demonstrated the increasing impact of plasma at higher Mach numbers. The study offered novel insights into the interactions between hypersonic plasma and electromagnetic waves, contributing to a broader understanding of hypersonic flight and its implications for RCS analysis.

Future works will extend the current analysis by investigating the effects of different body angles of attack on plasma formation and RCS (Radar Cross Section). Additionally, various frequencies and directions of the electromagnetic wave will be considered in the study of electromagnetic scattering.

Acknowledgments

This research was conducted under the financial support provided by the PON (Programmi Operativi Nazionali) research funds. We are grateful to the Italian Ministry of Education, University and Research (MIUR) for managing the PON funding program and for supporting our research endeavors.

References

[1] Bariselli, F., Boccelli, S., Magin, T., Frezzotti, A., and Hubin, A., "Aerothermodynamic modelling of meteor entry flows in the rarefied regime," *2018 Joint Thermophysics and Heat Transfer Conference*, 2018, p. 4180. https://doi.org/10.2514/6.2018-4180.

[2] Bariselli, F., Boccelli, S., Dias, B., Hubin, A., and Magin, T., "A self-consistent method for the simulation of meteor trails with an application to radio observations," *Astronomy & Astrophysics*, Vol. 641, 2020, p. A100. https://doi.org/10.1051/0004-6361/202037454.

[3] Anderson, J. D., *Hypersonic and high temperature gas dynamics*, Aiaa, 1989.

[4] Stix, T. H., *Waves in plasmas*, Springer Science & Business Media, 1992.

[5] Qian, J.-W., Zhang, H.-L., and Xia, M.-Y., "Modelling of Electromagnetic Scattering by a Hypersonic Cone-Like Body in Near Space," *International Journal of Antennas and Propagation*, Vol. 2017, No. Article ID 3049532, 2017, pp. 1–11. https://doi.org/https://doi.org/10.1155/2017/3049532.

[6] Gupta, R. N., Yos, J. M., Thompson, R. A., and Lee, K.-P., "A review of reaction rates and thermodynamic and transport properties for an 11-species air model for chemical and thermal nonequilibrium calculations to 30000 K," 1990.

[7] Park, C., "Review of chemical-kinetic problems of future NASA missions. I-Earth entries," *Journal of Thermophysics and Heat transfer*, Vol. 7, No. 3, 1993, pp. 385–398.

[8] Park, C., Jaffe, R. L., and Partridge, H., "Chemical-kinetic parameters of hyperbolic earth entry," *Journal of Thermophysics and Heat transfer*, Vol. 15, No. 1, 2001, pp. 76–90.

[9] Qian, J.-W., Zhang, H.-L., Xia, M.-Y., et al., "Modelling of electromagnetic scattering by a hypersonic cone-like body in near space," *International journal of antennas and propagation*, Vol. 2017, 2017.

[10] Chakravarthy, S., Peroomian, O., Goldberg, U., and Palaniswamy, S., "The CFD++ computational fluid dynamics software suite," *AIAA and SAE, 1998 World Aviation Conference*, 1998, p. 5564.

[11] Peroomian, O., Chakravarthy, S., Palaniswamy, S., and Goldberg, U., "Convergence acceleration for unified-grid formulation using preconditioned implicit relaxation," *36th AIAA Aerospace Sciences Meeting and Exhibit*, 1998, p. 116.

[12] Menter, F. R., "Improved two-equation k-omega turbulence models for aerodynamic flows," Tech. rep., 1992.

[13] Landau, L., Lifshits, E., and Pitaevskii, L., "Statistical physics, vol. 1980," , 1996.

[14] Scarabosio, A., Quijano, J. L. A., Tobon, J., Righero, M., Giordanengo, G., D'Ambrosio, D., Walpot, L., and Vecchi, G., "Radiation and Scattering of EM Waves in Large Plasmas Around Objects in Hypersonic Flight," *IEEE Transactions on Antennas and Propagation*, Vol. 70, No. 6, 2022, pp. 4738–4751. https://doi.org/10.1109/TAP.2022.3142310.

[15] Born, M., and Wolf, E., *Principles of optics: electromagnetic theory of propagation, interference and diffraction of light*, Elsevier, 2013.

[16] Kravtsov, Y. A., and Orlov, Y. I., *Geometrical optics of inhomogeneous media*, Vol. 38, Springer, 1990.

[17] Bremmer, H., and Lee, S., "Propagation of a geometrical optics field in an isotropic inhomogeneous medium," *Radio science*, Vol. 19, No. 01, 1984, pp. 243–257.

[18] Jin, J.-M., *Theory and computation of electromagnetic fields*, John Wiley & Sons, 2015.

[19] Dassault Systèmes, S., and Vélizy-Villacoublay, F., "CST Studio Suite 2019," 2019.

[20] Gnoffo, P. A., Johnston, C. O., and Thompson, R. A., "Implementation of radiation, ablation, and free energy minimization in hypersonic simulations," *Journal of Spacecraft and Rockets*, Vol. 47, No. 2, 2010, pp. 251–257.

[21] Bondeson, A., Rylander, T., and Ingelström, P., *Computational electromagnetics*, Springer, 2012.

[22] Gibson, W. C., *The method of moments in electromagnetics*, CRC press, 2021.